Solar Energy 184 (2019) 230–239

Contents lists available at ScienceDirect

Solar Energy

journal homepage: www.elsevier.com/locate/solener

Development of semi-transparent ZnO/FTO solar thermoelectric nanogenerator for energy efficient glazing

N.P. Klochko[a], K.S. Klepikova[a], V.R. Kopach[a], I.I. Tyukhov[b,*,1], V.V. Starikov[a], D.S. Sofronov[c,d], I.V. Khrypunova[a], D.O. Zhadan[a], S.I. Petrushenko[e], S.V. Dukarov[e], V.M. Lyubov[a], M.V. Kirichenko[a], A.L. Khrypunova[a]

[a] National Technical University "Kharkiv Polytechnic Institute", 2, Kirpichov St., 61002 Kharkiv, Ukraine
[b] San Jose State University, Department of Mechanical Engineering, One Washington Square, San Jose, CA 95192-0087, USA
[c] Institute for Single Crystals of NAS of Ukraine, 60, Nauky Ave., 61001 Kharkiv, Ukraine
[d] State Scientific Institution «Institute for Single Crystals» of NAS of Ukraine, 60, Nauky Ave., 61001 Kharkiv, Ukraine
[e] Kharkiv National University Named After V. N. Karazin, 4, Svobody Square, 61022 Kharkiv, Ukraine

ARTICLE INFO

Keywords:
Electrodeposition
1-D ZnO array
FTO
Solar thermoelectric nanogenerator
Glazing

ABSTRACT

In this work we developed and successfully tested a new design of semi-transparent solar thermoelectric nanogenerator (NG) based on the pulsed electrodeposited array of ZnO nanorods on transparent conducting fluorine doped tin oxide (FTO) substrate. An operation of this NG caused by a distinguishable temperature gradient between 1-D ZnO array and uncoated FTO that spontaneously created under heating of ZnO/FTO composition, including under the influence of sunlight. The developed NG combines benefits of low thermal emittance of FTO and ZnO coatings with TE technology for the harvesting of photo-thermal energy of outdoor sunlight by the windows themselves to produce electricity. The network of such NGs can be integrated harmoniously into buildings without affecting the overall aesthetics and serve as a source of electricity sufficiently high to make sensors entirely autonomous in energy by the harvesting solar near-infrared radiation and heat from ambient.

1. Introduction

A modern architecture, where a larger proportion of the exterior wall is designed and constructed with glass facades to be aesthetically pleasing and space efficient, but this also provides an additional challenge to its thermal efficiency. Untreated glass is a poor heat insulator whereby windows become a major heat transfer path between the inside and outside of buildings, resulting in unwanted heat transfer. Therefore the usage of energy efficient glazing is an important task (Liu et al., 2015; Fruh and Musleh, 2015; Anderson et al., 2016; Sarbu and Dorca, 2017; Ito et al., 2017; Prieto et al., 2017). Modern approaches are windows with low thermal emittance (Low-E) produced by depositing spectrally selective coatings on the glass surface, such as transparent conducting oxides, which maintain their transparency in solar wavelength (λ from 0.3 to 2.5 μm) and reflective in thermal radiation range (λ from 3.0 to 50 μm). According to Anderson et al. (2016), fluorine doped tin oxide (F-SnO_2 or FTO) is a high performing TCO material that has lower cost than indium tin oxide (ITO) and therefore it has been successfully used in recent years in Low-E glazing. Namely, FTO from Pilkington NSG TEC™ Glass of TEC 7 (7–8 Ω/sq) type is stable under atmospheric conditions, chemically inert, mechanically hard and abrasion tolerant, what is exclusively important for its use in energy-saving windows.

However, as it was reported by Anderson et al. (2016), Ito et al. (2017), He et al. (2018), the latest trends and research in energy efficient glazing applications are connected with a harvesting of photo-thermal energy of outdoor sunlight by the windows themselves to produce electricity, that could reduce the buildings external energy demand in an environmentally friendly manner. Modern active building window systems already used are new window designs that combine photovoltaic (PV) and thermoelectric (TE) technologies, in which an integrated or stand-alone PV systems or roof integrated PV panels investigated by Poulek et al. (2018) based on commercially available solar cells provide electricity to opaque bulk thermoelectric devices imbedded in a building structure near the glazing. As examples of such energy efficient glazing are solar thermoelectric cooling systems

* Corresponding author.
E-mail address: ityukhov@yahoo.com (I.I. Tyukhov).
[1] ISES member.

https://doi.org/10.1016/j.solener.2019.04.002
Received 7 March 2019; Received in revised form 28 March 2019; Accepted 1 April 2019

presented by Liu et al. (2015), Sarbu & Dorca (2017) and Prieto et al. (2017). At the same time, all these and other authors (Fruh and Musleh, 2015) have noted the complexity of the design and the insufficient efficiency of such systems, as well as the need to their improvement by means using semi-transparent solar cells and thin-film TE materials. Anderson et al. (2016) describe the benefits of incorporation of semi-transparent solar cells into window glazing potentially enabling visually pleasing building design in combination with power generation. To obtain semi-transparent solar cells for the building-integrated photovoltaics, different thin film technologies could be used, such as production of organic, perovskite and dye-sensitized solar cells. However, for such solar glazing to become a truly practical and realistic alternative they must be low cost, have high power conversion efficiency and long-term durability, and also be easy to manufacture. Because of unresolved challenges in the production of semi-transparent solar cells, that meet the above criteria, such energy efficient solar glazing is reviewed in accordance with Anderson et al. (2016) as still in its infancy.

As an alternative for solar cells in energy efficient windows authors Ito et al. (2017) proposed to use networks of small (1 mm in diameter) semi-transparent thin-film thermoelectric generators (TEGs), which would provide conversion of near-infrared (NIR) solar light into electricity. Every TEG contained small ball lens at a center of a pinhole. The ball lenses were used by Ito et al. (2017) to focus full solar light and to separate visible and NIR solar light using a chromatic aberration. The transmitted visible light, which passed through the transparent glass substrate, was used as daylight. The NIR light was defocused and irradiated the hot side of semicircular opaque thin-film thermoelectric elements, n-$Bi_2Te_{2.7}Se_{0.3}$ and p-$Bi_2Te_{2.7}Se_{0.3}$, with Cu contacts, which surrounded the hole. When solar light (AM1.5) irradiated at 298 K, the temperature gradient ΔT between the hot side of the center and the cold side of the circumference of the semicircular thermoelectric films was 0.58 K, the generated open circuit voltage of the single TEG was 0.88 mV, and maximum power equaled 1.0 nW. Set of the serially connected small TEGs generated specific open-circuit voltage and maximum power 4.5 V/m^2 and 51 μW/m^2, respectively. Such glazing equipped with set of small TEGs was expected to be used as an energy supply for Internet of Things sensors. Thus, in the work Ito et al. (2017), it was realized the energy efficient glazing due to thermoelectric conversion of solar energy using a network of many small TEGs, but with a rather complex design.

Nanogenerators (NGs), which can convert small-scale physical change into electricity, are emerging new technologies to harvest renewable energy from the environment that have attracted global attention (Yang et al., 2012a, 2012b; Norouzi et al., 2016; Jao et al., 2017; He et al., 2018; Tainoff et al., 2018). Recently, the most popular idea is to use of one-dimensional (1-D) nanostructures for the creation of TEGs and NGs as viable sources of power for autonomous wireless sensors (Yang et al., 2012a, 2012b; Zappa et al., 2014; Norouzi et al., 2016; Jao et al., 2017; He et al., 2018; Ishibe et al., 2018; Tainoff et al., 2018). Moreover, a photo-thermoelectric nanogenerator (PTENG) for infrared light harvesting proposed by He et al. (2018) is an interesting approach to solving the problem of energy efficient glazing. This PTENG is based on plastic thermoelectric nanocomposite strip made of poly (3,4-ethylenedioxythiophene) polystyrene sulfonate (PEDOT:PSS) matrix and tellurium (Te) nanowires as a filler (Te/PEDOT nanocomposite film). A pair of thin-film electrodes made of silver paste deposited on the ends of the strip. To create temperature difference ΔT along the thermoelectric Te/PEDOT strip length, which acted as driving force of the thermoelectric nanogenerator, a photothermal layer contained molybdenum disulfide nanoclusters in a polyurethane matrix (MoS_2/PU) was applied to one end of the strip. This MoS_2/PU layer heated under sunlight and thereby heat the one end of the Te/PEDOT film creating ΔT. As an experiment showed by He et al. (2018), ten thin film PTENGs with dimensions of 1 × 3 cm each delivered an output voltage of 1.48 mV by harvesting photo-thermal energy of outdoor sunlight at an atmospheric temperature of 20 °C. Unfortunately, the Te/PEDOT film had a yellow color, and on two thirds of its area there were dark opaque Ag electrodes and MoS_2/PU layers, therefore the device as a whole was not transparent enough for the glazing. Thermoelectric nanogenerator network of Tainoff et al. (2018) made through MEMS technology using opaque silicon plate and suspended silicon nitride membranes with n-Bi_2Te_3 and p-Bi_2Te_3 nanorods as thermoelectric legs. Since membranes have a negligible mass, their temperature was free to fluctuate contrary to the bulk silicon frame that conducts well the heat. Thus, a temperature gradient appeared between the membranes and the bulk silicon frames when the whole setup submitted to a heat source (hot air flow, radiation, etc.). Standard MEMS technique enabled Tainoff et al. (2018) to obtain array of thousands of membranes, each generated around 0.3 nW power for ΔT = 8 K, which can lead to power production of up to 750 μW for 10 cm^2 area, a value sufficiently high to make sensors completely autonomous in energy. However, this NGs network design is not suitable for glazing due to its opacity. Similarly, completely opaque and therefore unsuitable for glazing is thermoelectric nanogenerator fabricated by Jao et al.(2017) based on thin-film nanocomposite of silver telluride (Ag_2Te) nanowires in the PEDOT:PSS matrix with top Ag electrode and bottom Al electrode with 3 × 1.5 cm dimensions that can provide an output voltage of 2.6 mV at a temperature difference of 25 °C.

Many researchers have used semi-transparent 1-D ZnO to create NGs (Yang et al., 2012a, 2012b; Norouzi et al., 2016), as it is recognized as an effective thermoelectric material (Zappa et al., 2014; Ishibe et al., 2018; Klochko et al., 2018a; Matsuo et al., 2018). Authors Yang et al. (2012a) presented a transparent thermoelectric nanogenerator based on single Sb-doped ZnO micro/nanobelt (600 nm wide and with length of larger than 3 mm) synthesized by chemical vapor deposition method. The ZnO micro/nanobelt placed on the glass substrate, and two ends of the micro/nanobelt were fixed tightly by the silver paste on the substrate in a way that the distance between the two electrodes was 3 mm. A thin poly (dimethylsiloxane) layer used to package the device to avoid the effect of atmosphere and to prevent Sb-doped ZnO micro/nanobelt from contamination or corrosion. Under a temperature difference between two electrodes ΔT = 30 K, the NG produced an output voltage of about 10 mV and an output current of 194 nA. However, the manufacturing technology of the nanogenerators based on single ZnO micro/nanobelts (Yang et al., 2012a) is not acceptable for mass production, and therefore is not suitable for glazing. Yang et al. (2012b) have shown semi-transparent 1-D ZnO array obtained via hydrothermal method on ITO substrate as a common bottom electrode for a direct 1-D ZnO connecting to an external circuit, and with a silver film deposited on the top of ZnO, which served as a common top Schottky contact. Nevertheless, this device proposed by Yang et al. (2012b) to use as pyroelectric nanogenerator for harvesting thermal energy from a time-dependent temperature fluctuation to convert wasted energy into electricity for powering nanodevices. Norouzi et al. (2016) described a thermoelectric energy harvesting using an array of vertically aligned Al-doped ZnO nanorods. 1-D ZnO arrays hydrothermally grown on the glass or on the silicon substrate covered by 250-nm layer of titanium and a 350-nm-thick layer of gold as a bottom contact. To prevent possible short-circuiting between the bottom and the top Ti/Au electrodes the gaps among ZnO nanorods filled with photoresist. Output voltage under a temperature difference of 1 K between two contacts was up to 0.1–0.28 mV, and the generated current owing to a summation of the currents from individual nanorods grown in an array structure reached 1 μA or 3.5 μA on glass and on silicon substrates, correspondingly. The thermoelectric NG have been introduced by Norouzi et al. (2016) as a device for energy harvesting from the waste heat in the living environment, and due to Ti/Au electrodes opacity it is not suitable for the glazing. However, the idea to apply 1-D ZnO arrays used as the basis for the new design of solar thermoelectric nanogenerator for energy efficient windows that we developed and present in this study.

A physical effect for the new design of a vertical (out-of-plane) type thermoelectric NG presented in this work consists in a spontaneous

temperature gradient ΔT of several Celsius degrees between FTO surface and upper ends of 1-D ZnO arrays on FTO substrate, which arises under influence of thermal radiation including due to outdoor sunlight. For the harvesting energy from solar heat, the power generation densities and fabrication costs of TEGs considered more important than their conversion efficiency because this energy essentially obtained free of charge (Zhan et al., 2018). Therefore, we used electrodeposition of 1-D ZnO arrays as simple and potentially industrially scalable process with low maintenance and set-up costs (Matsuo et al., 2018). Moreover, according to Matsuo et al. (2018), electrochemical deposition is suitable to form thermoelectric micro-devices using combination of lithography techniques due to its selective deposition together with low reaction temperature and process simplicity. The solar thermoelectric NG design developed by us combines benefits of low thermal emittance of FTO and ZnO coatings with TE technology for the harvesting of photo-thermal energy of outdoor sunlight by the windows themselves to produce electricity. In the developed design of ZnO/FTO solar thermoelectric NG we used only one type of semiconductors, similarly to (Yang et al., 2012a; Norouzi et al., 2016; Jao et al., 2017; He et al., 2018; Zhan et al., 2018). Namely, we used exclusively 1-D ZnO arrays of *n*-type conductivity that greatly simplifies the device design compared with the use of thermocouples as in (Zappa et al., 2014; Matsuo et al., 2018). A network of the developed semi-transparent nanogenerators can be located directly on the inner surface of the Low-E windows to serve as an electricity source by the harvesting an NIR energy of outdoor sunlight and heat from ambient, and will be integrated harmoniously into buildings without affecting the overall aesthetics.

2. Experimental procedures

As substrates, we used 2 × 3 cm plates of fluorine doped tin oxide (TEC 7 from Pilkington NSG TEC™). Nanostructured 1-D ZnO arrays were obtained on FTO surface in accordance with Klochko et al. (2018b) by cathodic electrochemical deposition using a standard thermostatic three-electrode electrochemical cell with platinum spring as counter-electrode and saturated Ag/AgCl reference electrode in unstirred aqueous electrolyte containing 0.01 M $Zn(NO_3)_2$ and 0.1 M $NaNO_3$. Temperature of the electrolyte was 70 °C. Firstly, ZnO seed layers were formed via potentiostatic electrochemical deposition provided by a programmable impulse potentiostat "PI-0.5–1.1" during short time (30 s) at potential $U = -1.3$ V (here and below, vs. Ag/AgCl). After that, a plating of 1-D ZnO arrays carried out in the same electrolyte during from 15 to 30 min in the pulsed mode by applying rectangular potential pulses. The lower and upper potential limits were, respectively, $U_{off} = -0.7$ V and $U_{on} = -1.3$ V. A duty cycle ($D_c = 0.4$) was given as relation $T_{on}/(T_{on} + T_{off})$, where T_{on} is a time at potential U_{on}, and T_{off} is a time at potential U_{off}. Pulse frequency f was 2 Hz. As a result, 1-D ZnO arrays homogeneous over the sample area with average thickness (t), which corresponds to the length of nanorods in the 0.9–1.1 μm range grown on FTO surfaces.

Morphology of 1-D ZnO arrays and uncoated FTO surface observed by scanning electron microscopy (SEM) in a secondary electron mode. The SEM instrument "Tescan Vega 3 LMH" operated at an accelerating voltage 30 kV without the use of additional conductive coatings.

Elemental analysis of FTO and 1-D ZnO array was carried out by X-ray fluorescence (XRF) microanalysis using an energy dispersive spectrometry (EDS) system "Bruker XFlash 5010". Energy dispersion spectra taken from the 50 × 50 μm^2 sample areas. Quantification of the spectra carried out in the self-calibrating detector mode.

Optical transmission $T_o(\lambda)$ of FTO substrate and 1-D ZnO arrays were recorded in the UV–Vis-NIR range with an "SF-2000" spectrophotometer. FTO substrates used as control samples when transmittance spectra of 1-D ZnO arrays recorded. Infrared transmission spectra for FTO substrate and for the electrodeposited 1-D ZnO arrays on FTO were obtained using Fourier transform infrared spectroscopy (FTIR) method with a Fourier spectrophotometer SPECTRUM ONE (PerkinElmer) in the 400–4000 cm^{-1} range (at wavelengths from 2.5 to 25 μm) and at a resolution of 1 cm^{-1} at room temperature. In addition, for infrared studies by means of FTIR spectroscopy we used tablets with potassium bromide (KBr) filler. For this, 1-D ZnO particles scraped off the FTO substrate surface with a scalpel, and then mixed with KBr, triturated and tableted.

To analyze phase composition, structural and substructural parameters of 1-D ZnO arrays, we recorded X-ray diffraction (XRD) patterns by a "DRON-4" diffractometer. Scanning performed with Bragg–Brentano focusing (theta – 2 theta). The resulting XRD patterns processed and the profile parameters of the diffraction lines calculated by "New-Profile v.3.4 (486)" and "OriginPro v.7.5" software. The presence of crystalline phases revealed by comparing the experimental diffraction patterns with the reference database JCPDS by using PCPDFWIN v.1.30 software. In accordance with Zak et al. (2011) and Kahouli et al. (2015), to evaluate micro-strains $\varepsilon = \Delta d/d$ (where d is the crystal interplanar spacing according to JCPDS, and Δd is the difference between the corresponding experimental and reference interplanar spacings) we applied the X-ray line broadening method using the Scherrer equation and the Williamson-Hall approximation. Dislocation density was evaluated as $1/D^2$ according to Dongol et al. (2015), where D is the average crystallite size. The crystal lattice constants, a and c, of the 1-D ZnO grains were calculated from the positions of the pairs of adjacent to each other indexed lines in the X-ray diffraction patterns by the Nelson–Reilly graphical extrapolation method and refined using the least-squares method (LSM) by UnitCell software on the basis of all recorded reflections in the X-ray diffraction patterns, as in Kopach et al. (2016). Texture quality of 1-D ZnO array estimated by the Harris method (Kopach et al., 2016; Klochko et al., 2018c). Pole density P_i, which determines an axis of the crystal plane that is oriented normal to the surface, calculated according to the equation (Kopach et al., 2016; Klochko et al., 2018c):

$$P_i = (I_i/I_{0i})/\left[1/N \sum_{i=1}^{N} (I_i/I_{0i})\right], \tag{1}$$

where I_i, I_{0i} are integral intensity of the i-th diffraction peak of the film and etalon, respectively; N is the number of lines presented in the diffraction. Texture axis has the index, which corresponds to the largest value of P_i. The orientation factor f for the relevant direction calculated from the formula (Klochko et al., 2018c):

$$f = \sqrt{1/N \sum_{i=1}^{N} (P_i - 1)^2}. \tag{2}$$

Schematic illustration of the developed semi-transparent ZnO/FTO solar thermoelectric nanogenerator based on 1-D ZnO array on FTO substrate, and two setups for its characterization are presented in Fig. 1. Fig. 1(a) on the right shows a schematic design of our NG consisted of FTO plate partially covered by 1-D ZnO array with ohmic aluminum (Al) banded contacts fabricated on FTO and on the tops of zinc oxide nanorods. In the process of the NG test sample creating, Al vacuum deposition carried out at 25° angle to the substrates on limited areas of FTO and 1-D ZnO through a shadow mask in order to avoid a shunting. Then, conductive adhesive with silver filler applied to the Al surface for providing galvanic contacts with copper microwires. Temperature gradient ΔT between 1-D ZnO and uncoated FTO substrate was created using hot plate of the Peltier element "TEC1-12730", on which test sample ZnO/FTO without Al contacts or test sample of the developed thermoelectric NG was located as it shown in Fig. 1(a) on the left. Temperature distributions over the heated area, including ΔT between 1-D ZnO and uncoated FTO substrate, fixed and measured by an infrared camera "FLUKE Ti10". Fig. 1(b) shows schematic setup for a measuring of output characteristics of NG test samples under illumination of 1500 W halogen lamp with reflector "Philips Plusline L1CT/10" or under artificial solar lighting AM1.5G normalized to 1000 W/m^2,

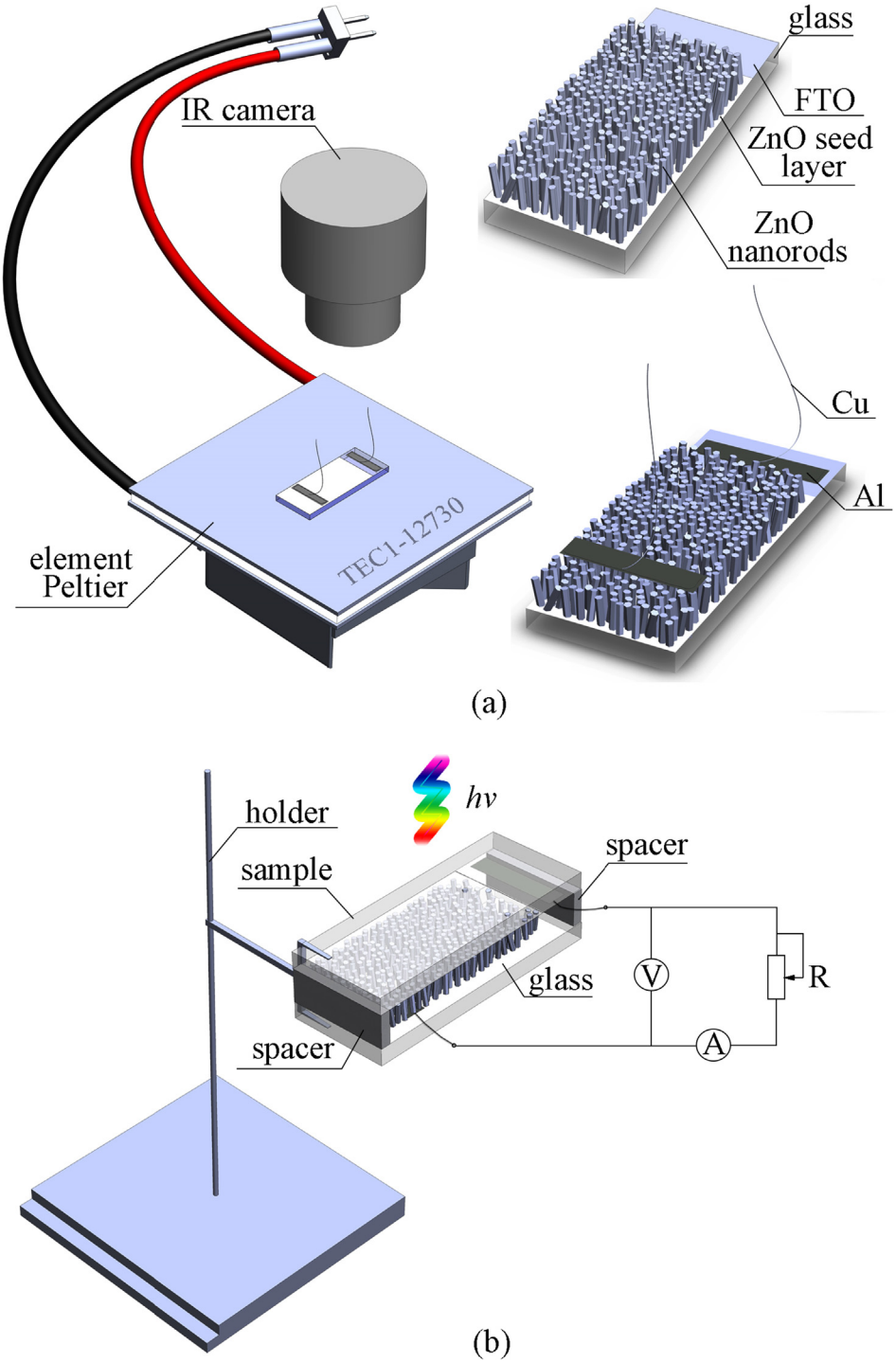

Fig. 1. Schematic illustration of the developed semi-transparent ZnO/FTO solar thermoelectric NG and two setups for its characterization. (a) – Setup for a measuring of temperature distribution over the heated NG area (on the left) and schematic design of NG without and with Al contacts (on the right). (b) – Setup for a measuring of output characteristics of NG under imitated solar illumination (R – variable resistor as a load, V – voltmeter for a measuring of output voltage V_{out}; A – microamperemeter for a measuring of output current I_{out}).

which created using a homemade solar simulator. In Fig. 1 (b), the NG fixed in a holder so that the 1-D ZnO array is at the bottom, and the light enters the 1-D ZnO array through the FTO plate from glass side. A clean glass plate fixed under the nanogenerator at a distance of 4 mm from the 1-D ZnO array using a spacer. Thus, Fig. 1(b) simulates glazing.

3. Results and discussion

Fig. 2 shows top view SEM images of the electrodeposited array of vertically aligned ZnO nanorods with diameters about 300 nm and with typical hexagonal tops, and also of the uncoated FTO substrate. Data about 1-D ZnO array phase composition obtained from X-ray diffractions presented in Fig. 3(a). Analysis of XRD patterns in Fig. 3(a) has shown that both electrodeposited 1-D ZnO arrays used in NG test samples, which t equals 0.9 or 1.1 μm, are single-phased, polycrystalline

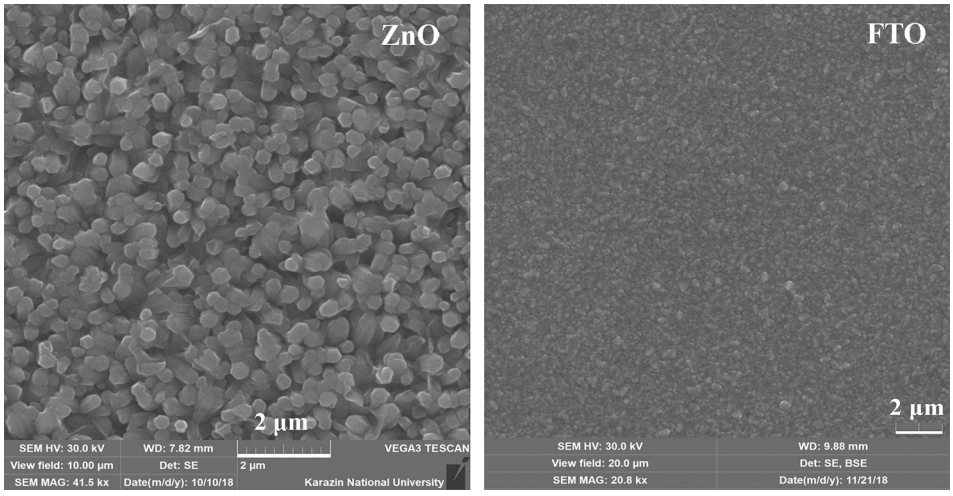

Fig. 2. Top view SEM images of the electrodeposited 1-D ZnO array on FTO substrate (on the left) and of the uncoated FTO substrate (on the right).

in nature and matching with hexagonal wurtzite structure ZnO (JCPDS 36-1451). Calculations of the structural parameters have revealed (Table 1) the ZnO average crystallite sizes D above 100 nm with dislocation density $\sim 1 \times 10^{14}$ lines/m^2 and small micro-strains. It was found a preferential orientation along to the ⟨0 0 1⟩ direction (the orientation factor in the (0 0 2) plane f from 0.95 up to 1.44 a.u.), which is characteristic for the 1-D ZnO nanostructures.

XRF data in Fig. 3(b) have shown chemical composition of ZnO nanorods in ZnO/FTO test sample obtained by pulsed electrochemical deposition of 1-D ZnO arrays on FTO substrate, and also chemical composition of the uncoated FTO substrate. Calcium and silicon in both XRF spectra are components of glass. The presence of carbon can be evidence of unavoidable pollution with organic matter, as well as adsorption of carbon dioxide from the atmosphere. The excess oxygen content in the XRF spectra can be explained both by its presence in silicate glass, and by the adsorption of water and oxygen on the large specific surface of the zinc oxide nanorods.

Dependences of the optical transmittance on the wavelength in the UV–Vis-NIR range, which are shown in Fig. 4(a), are typical for 1-D ZnO arrays electrodeposited in the pulsed mode (Klochko et al., 2018b). As seen in Fig. 3(a), the visible transmittance of the thinner 1-D ZnO array reaches ~70%, and T_o naturally decreases with 1-D ZnO array thickness t to ~50%, that is, T_o is reduced with a growing of the zinc oxide nanorod length. Nevertheless, both 1-D ZnO arrays are semi-transparent almost in a whole Vis-NIR solar spectra range. Data of $T_o(\lambda)$ obtained by means of FTIR spectra for FTO substrate and for 1-D ZnO array on FTO surface show (Fig. 4(b)) that FTO substrate, and also ZnO/FTO compositions for the developed semi-transparent solar thermoelectric NG are translucent for the NIR solar spectrum and absolutely opaque at λ above 3 μm. In other words, Fig. 4(a) and (b) show that 1-D ZnO arrays absorb Mid-Infrared (MIR) radiation and a certain amount of NIR radiation from the sun in the 780–3000 nm range better than the uncoated FTO.

Accurate data concerning zinc oxide absorption in the MIR region obtained using Fourier transform infrared spectroscopy. FTIR spectrum of the KBr supported 1-D ZnO tablet in Fig. 4(c) has some absorption peaks. We observed two ZnO-related absorption peaks centered at 436.3 cm^{-1} and at 542.6 cm^{-1}. According to Kooti and Naghdi Sedeh (2013) and Sowri Babu et al. (2013), a strong peak at 436 cm^{-1} is attributed to the stretching vibrations of Zn—O bonds. However, there are various interpretations in the literature relative to the absorption at 542.6 cm^{-1}, since as stated in Sowri Babu et al. (2013), FTIR spectrum of zinc oxide is sensitive to variations in ZnO particle size, shape and morphology, and the position of the peaks is dependent on axial ratio (c/a) of the ZnO nanocrystals. We took into account that in accordance with Soni et al. (2013), an absorption band around 520 cm^{-1} is the typical characteristic band of the wurtzite hexagonal phase pure ZnO. As noticed by Xiong et al. (2006), the band at 505 cm^{-1} may be associated with oxygen deficiency and/or oxygen vacancy (V_O) defect complex in ZnO. Thus, because of the nanocrystalline structure of the electrodeposited ZnO nanorods, we assume that both above estimates may be used to interpret FTIR spectrum recorded by us at 542.6 cm^{-1}.

According to a large number of researches (Morishige et al., 1980; Xiong et al., 2006; Sowri Babu et al., 2013; Soni et al., 2013; Kumar and Rani, 2013; Kooti and Naghdi Sedeh, 2013; Kahouli et al., 2015), the most intensive broad absorption peak which is centered in FTIR of the KBr supported 1-D ZnO tablet at 3435.6 cm^{-1} corresponds to the hydroxyl group OH. As indicated by Morishige et al. (1980); Xiong et al. (2006); Sowri Babu et al. (2013); Soni et al. (2013); Kumar and Rani (2013), this hydroxyl peak is due to O—H stretching and may come from the surface adsorption of ambient water. In accordance with (Sowri Babu et al., 2013; Kahouli et al., 2015), absorption peak at 1633.8 cm^{-1} corresponds to bending mode of the adsorbed water or to organic species, for example, unavoidable pollution from the environment, which XRF data showed. However, quoting (Kumar and Rani, 2013), absorption peak at 1633.8 cm^{-1} is corresponding to Zn—O stretching, and absorption peak at 1116.0 cm^{-1} may be due to O-H deformation. Inevitable organic pollution, which we registered by XRF, explains an appearance of absorption peaks at 1462.9 cm^{-1}, 1034.9 cm^{-1} and near 2900 cm^{-1} (Sowri Babu et al., 2013). So, as seen in Fig. 4(c), Mid-Infrared radiation is absorbed by 1-D ZnO surface mostly because it is coated with organic and inorganic species. In this way, there is an important conclusion from our FTIR investigations, which is associated with a high adsorption capacity of the electrodeposited 1-D ZnO due to its large specific surface. When water and other organic and inorganic substances on the 1-D ZnO surface absorb infrared radiation, this causes the energy increase through an exciting of O—H stretching and other vibrations. The above phenomenon can manifest itself in a greater heating of 1-D ZnO array in ZnO/FTO compared to uncoated FTO, including in NG test samples, thereby ensuring their functioning as semi-transparent solar thermoelectric NGs. Note, that NIR solar illumination with λ = 2.9 μm (i.e., with wave number 3435.6 cm^{-1}) have exactly such energy as the most intensive absorption peak in the 1-D ZnO FTIR spectrum.

Fig. 5 shows well distinguishable temperature gradients ΔT between 1-D ZnO array and uncoated FTO that are spontaneously created under a heating of ZnO/FTO compositions as shown in Fig. 1(a) using the Peltier element up to temperatures in the range of 29.3–35.3 °C. In addition, Fig. 5 shows photos of the corresponding ZnO/FTO samples with and without aluminum contacts. It can seen that ΔT increases with

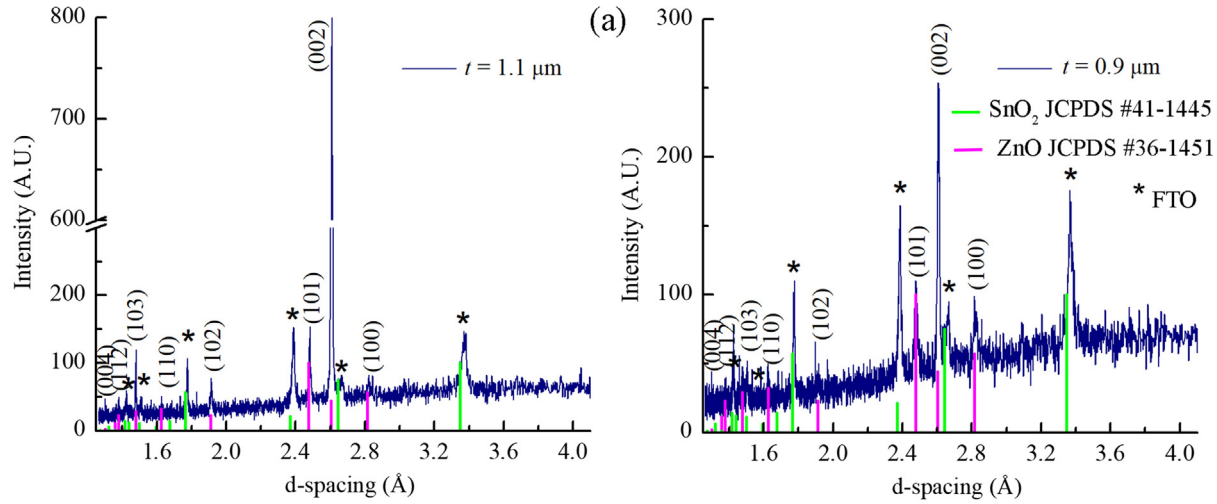

Element	At. No.	Netto	Mass [%]	Mass Norm. [%]	Atom [%]	abs. error [%] (1 sigma)	rel. error [%] (1 sigma)
C	6	422	4.09	4.79	12.90	1.23	30.07
O	8	6476	25.26	29.60	59.84	3.81	15.07
Si	14	1823	1.00	1.18	1.35	0.08	8.01
Ca	20	4157	1.69	1.98	1.59	0.08	4.94
Zn	30	30722	28.03	32.85	16.25	0.73	2.60
Sn	50	44677	25.26	29.60	8.07	0.79	3.11
		Sum	85.33	100	100		

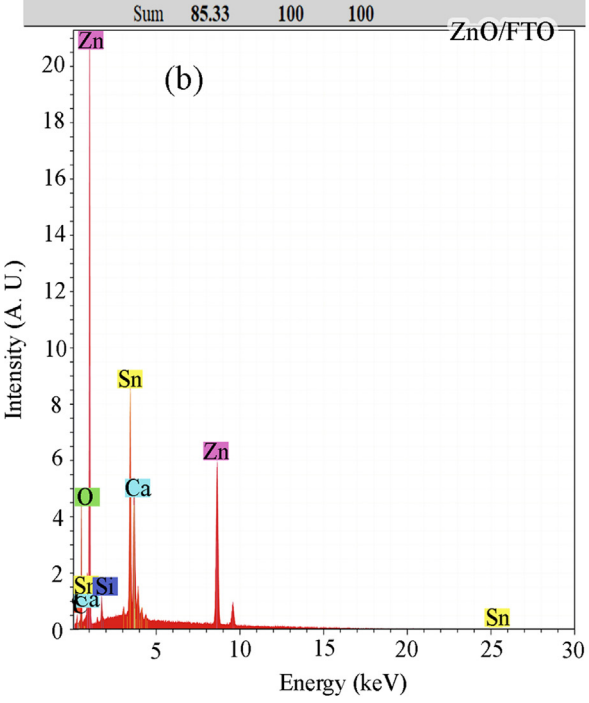

Element	At. No.	Netto	Mass [%]	Mass Norm. [%]	Atom [%]	abs. error [%] (1 sigma)	rel. error [%] (1 sigma)
Sn	50	79075	39.01	42.96	9.30	1.19	3.06
O	8	4437	26.63	29.33	47.11	4.29	16.10
C	6	1602	14.33	15.78	33.77	2.89	20.17
Si	14	21106	7.18	7.91	7.24	0.35	4.90
Ca	20	9560	3.65	4.02	2.58	0.14	3.86
		Sum	90.80	100	100		

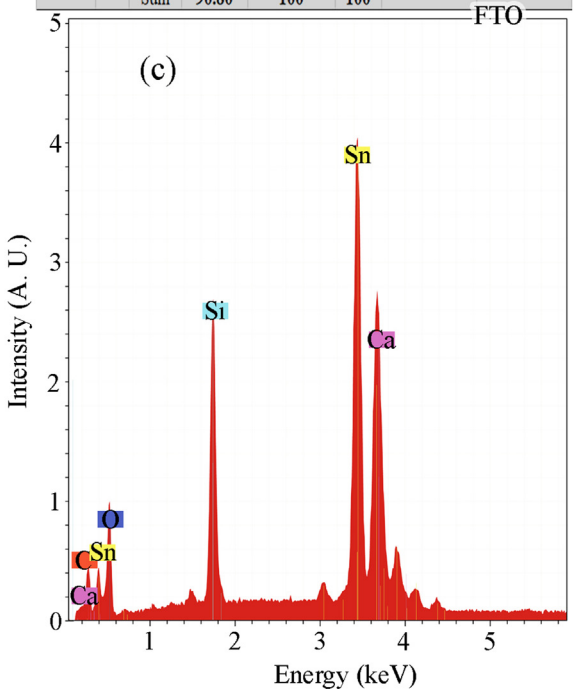

Fig. 3. (a) – XRD patterns of the electrodeposited in the pulsed mode 1-D ZnO arrays used in NG test samples; (b) and (c) – XRF data, which shown chemical composition of ZnO nanorods and uncoated FTO substrate, respectively, as the basis of semi-transparent ZnO/FTO solar thermoelectric NG test samples.

the heating of the external surface of the glass both in the ZnO/FTO composition without Al contacts, and also in the thermoelectric NG test sample. Besides, ΔT increases with the 1-D ZnO array thickness. The infrared images in Fig. 5(b) and a graph in Fig. 5(c) demonstrate an increase of ΔT between 1-D ZnO array and uncoated FTO substrate in ZnO/FTO NG test sample with $t = 0.9\,\mu m$ up to 3.2 °C, when the temperature of the hot plate of the Peltier element reaches 35.3 °C.

As it was revealed by hot probe measurements in (Klochko et al., 2015), electrodeposited 1-D ZnO arrays have *n*-type conductivity. A measuring of output parameters of the developed semi-transparent ZnO/FTO solar thermoelectric NG under imitated AM1.5G illumination, or when it illuminated with the halogen lamp using setup in Fig. 1(b), has revealed an accumulation of positive charge on the 1-D ZnO array surface. Before measurements of output characteristics of the NG test sample, the sample illuminated for half an hour using a solar simulator. As a result, the average temperature of the nanogenerator increased to 30 °C when using AM1.5G, and to 50 °C when illuminated by the halogen lamp (the temperature in the room where the tests carried out was 16 °C). Fig. 6 shows output characteristics for two test samples of semi-transparent ZnO/FTO solar thermoelectric NGs with $t = 0.9\,\mu m$ and $t = 1.1\,\mu m$. It can be seen in Fig. 6(a) that output characteristics of the developed semi-transparent ZnO/FTO

Table 1
Structural parameters of the pulsed electrodeposited 1-D ZnO arrays on FTO substrates.

1-D ZnO array thickness t, μm	Crystallite size D, nm		Micro-strains ε, 10^{-3} a.u.		Lattice parameters, Å				Texture		
					Nelson–Reilly method		LSM				
	According to Scherrer	Accor ding to Williamson-Hall	According to Scherrer	According to Williamson-Hall	a	c	a	c	hkl	P_{hkl}	f, a.u.
Etalon ZnO (JCPDS #36-1451)	–	–	–	–	3.249	5.206	3.249	5.206	–	–	–
t = 0.9	120	70–140	1.1	0.1–0.8	3.251 ± 0.005	5.220 ± 0.005	3.255 ± 0.005	5.218 ± 0.005	(0 0 2)	3.2	0.95
t = 1.1	240	from 120 to > 200	0.5	0.6–1.1	3.260 ± 0.005	5.213 ± 0.005	3.260 ± 0.005	5.216 ± 0.005	(0 0 2)	4.4	1.44

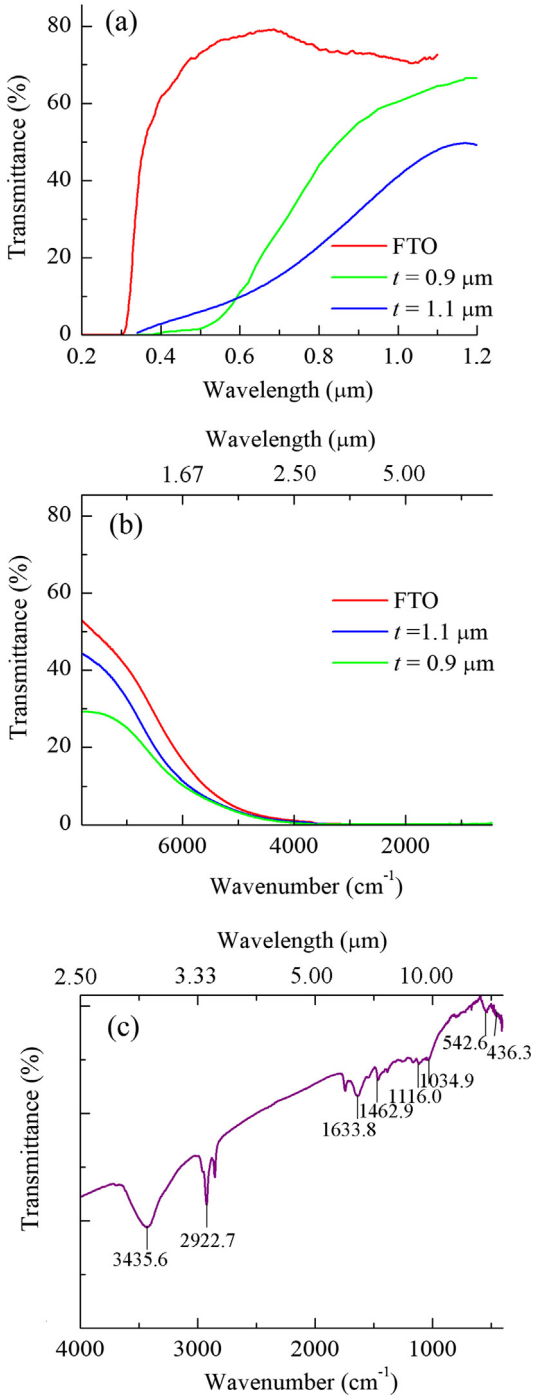

Fig. 4. (a) – Transmittance spectra in the UV–Vis-NIR range of FTO substrate and two 1-D ZnO arrays with different length of nanorods t; (b) – infrared transmittance spectra for FTO substrate and for these 1-D ZnO arrays on FTO substrate; (c) – FTIR spectrum of the KBr supported 1-D ZnO tablet.

thermoelectric NG at AM1.5G illumination are following: open circuit voltage V_{oc} = 0.065 mV, short current I_{sc} = 11 nA, and maximum output power P_{max} = 0.17 pW. When the average temperature of the nanogenerator increased up to 50 °C, it was observed a significant improvement in the output characteristics of the nanogenerators, which in accordance with Fig. 5(c) can be explained by an increase in the temperature gradient ΔT with NG heating. In addition, the resistance of 1-D ZnO naturally decreases with temperature, which also shown experimentally (Klochko et al., 2015). As seen in Fig. 6(b), the same NG test sample irradiated with the halogen lamp, accompanied by heating the

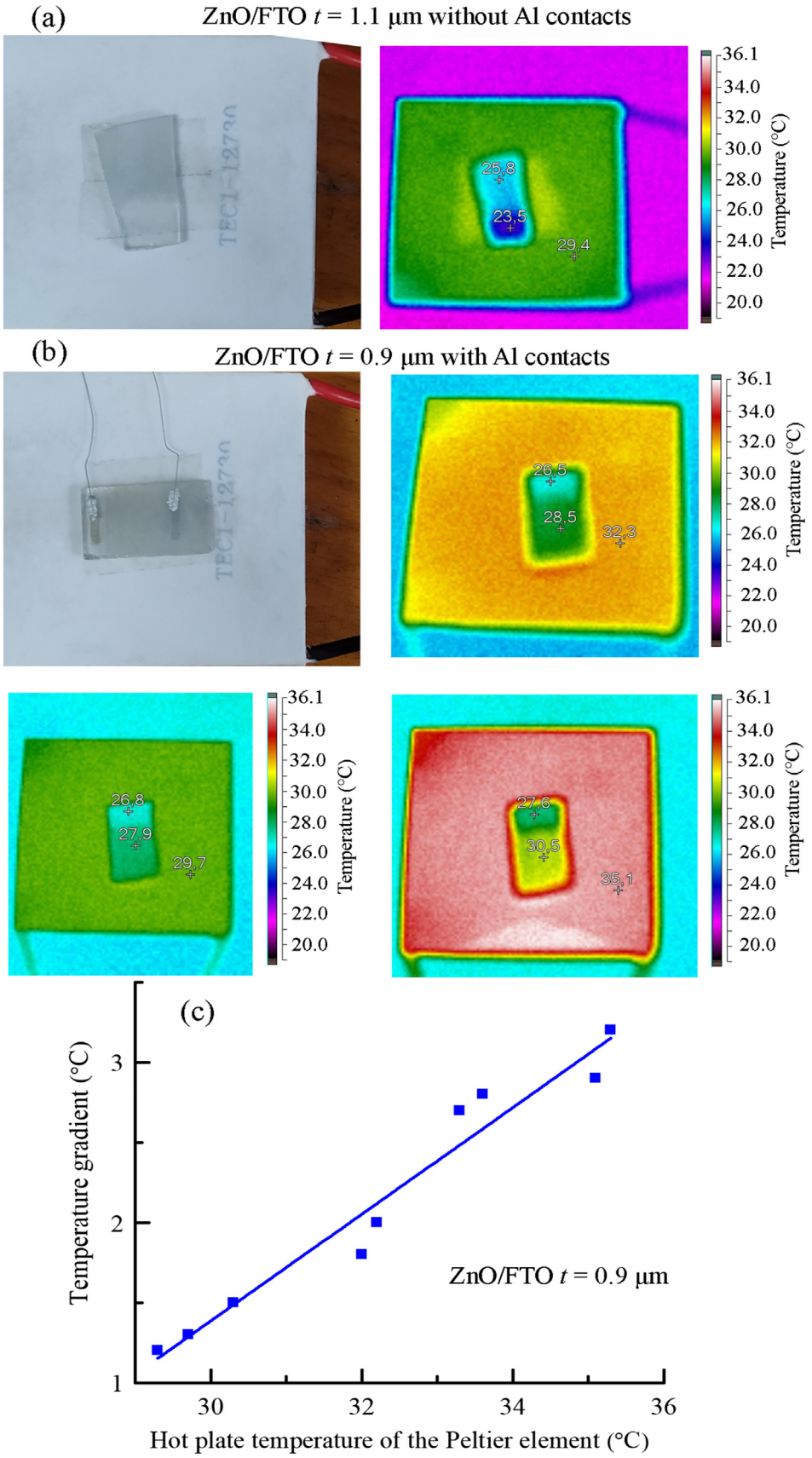

Fig. 5. (a) – Photo and infrared image taken during heating with the Peltier element as shown in Fig. 1 (a) for ZnO/FTO sample with t = 1.1 μm and without Al contracts. (b) – Photo and three infrared images taken during heating to different temperatures with the Peltier element as shown in Fig. 1 (a) for ZnO/FTO NG test sample with t = 0.9 μm and with Al contracts. (c) – Dependence of the temperature gradient ΔT between 1-D ZnO and uncoated FTO substrate in ZnO/FTO NG test sample with t = 0.9 μm, on the temperature of the Peltier element hot plate.

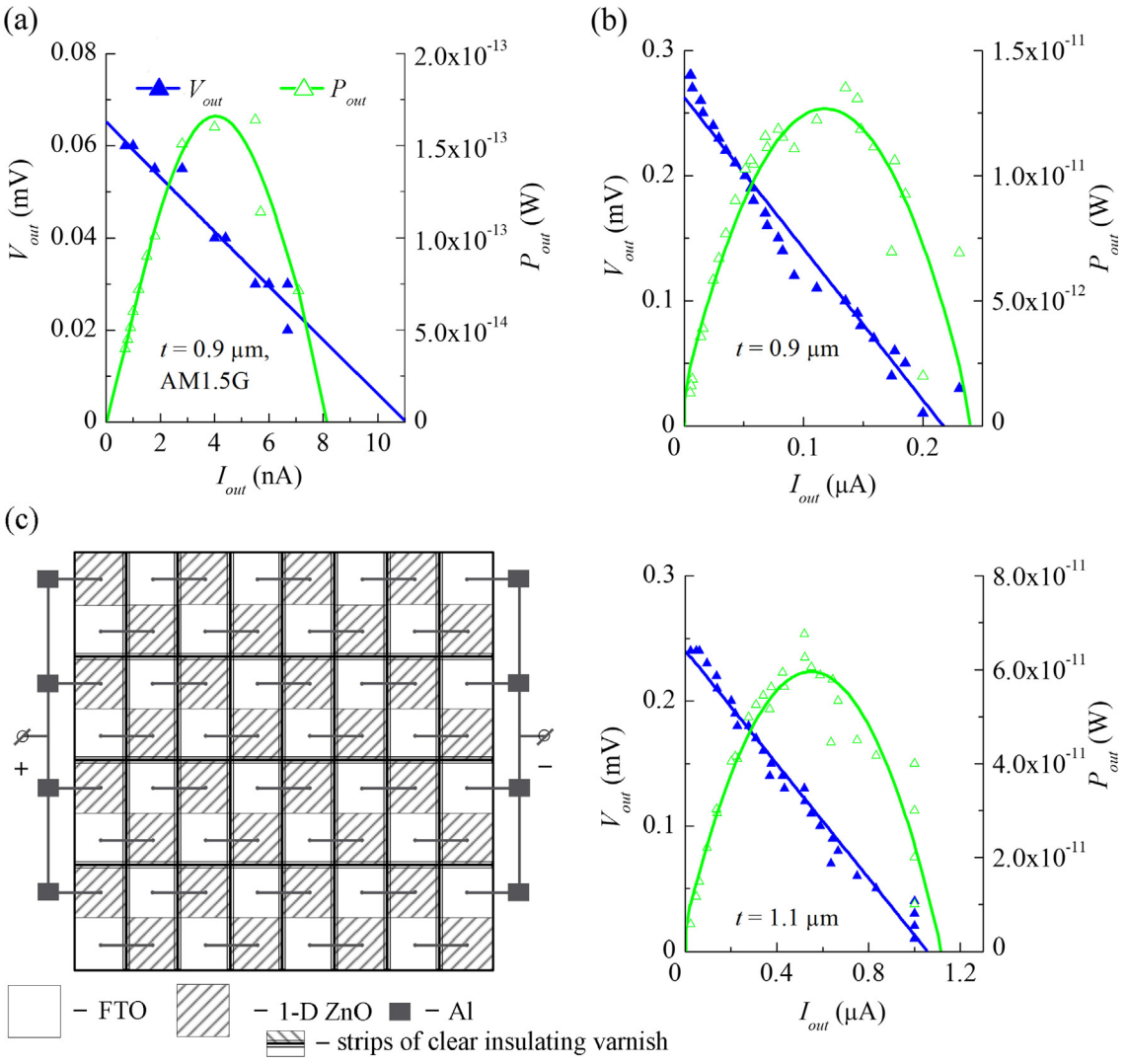

Fig. 6. Output voltage V_{out} (solid triangles) and output power P_{out} (opened triangles) versus output current I_{out} for test samples of semi-transparent ZnO/FTO solar thermoelectric nanogenerator with different length of nanorods t: (a) – at imitated solar illumination AM1.5G, average NG temperature 30 °C, t = 0.9 μm; (b) – at illumination by the halogen lamp, average NG temperature 50 °C (t = 0.9 μm for upper graph, t = 1.1 μm for lower graph). (c) – Schematic illustration of the proposed design for a network of semi-transparent ZnO/FTO solar thermoelectric NGs.

NG to the average temperature of 50 °C, showed the following output characteristics: V_{oc} = 0.28 mV, I_{sc} = 220 nA, and P_{max} = 13 pW. Also it can be seen in Fig. 6(b) that the elongation of nanorods to t = 1.1 μm provided a further increase in the efficiency of the thermoelectric nanogenerator, which can be explained by an increase in the temperature gradient with t increasing in Fig. 5. For this case, the output NG test sample characteristics are V_{oc} = 0.24 mV, I_{sc} = 1.1 μA, and P_{max} = 60 pW.

Fig. 6(c) proposes a design of a network consisting of 32 semi-transparent ZnO/FTO solar thermoelectric nanogenerators, which can be fabricated using the lithography and film deposition processes. For the NG network production, arrays of zinc oxide must be electrodeposited simultaneously on non-isolated areas of the big FTO plate. After taking out from the bath, washing and drying, the boundaries of the ZnO/FTO areas on the FTO plate, which are marked in Fig. 6(c) by thick lines, must be etched or FTO film on these boundaries must became non-conductive, for example, by means of laser beam. After that, it is necessary to apply clear insulating varnish strips on these boundaries. Then line contacts and areas marked in Fig. 6(c) with black applied with aluminum film in vacuum through a shadow mask. Due to the presence of non-conductive lacquer stripes, the Al contacts should connect the areas of 1-D ZnO and FTO with different temperatures. An important technological step is to check the possible defects and non-uniformity of characteristics of the semi-transparent ZnO/FTO solar thermoelectric NGs, from which the network assembled. For this purpose, the laser scanning technique proposed by Litvinenko et al. (2000) for a dynamical optical reflectance thermography will be used.

According to calculations, when using the design presented in Fig. 6(c), the output current of the NG network will increased up to four times as compared with I_{out} of single NG, and the output voltage will be up to eight times compared to V_{out} of the single nanogenerator. Accordingly, the output power, ideally, can exceed the power of a single nanogenerator by as many times as the network contains NGs. In reality the output power will be less, however the number of nanogenerators in the network may be much larger, including a covering the entire area of the glazing. Note, that I_{out} produced by the network of the NGs is regulated by a changing the area of the opaque aluminum contacts, especially those Al pads that are deposited on the tops of 1-D ZnO. The larger the Al contact area, the greater the current, and the less transparency. Thus, it is very important that there is a trade-off between the amount of light passing through the glazing with semi-transparent NGs located directly on the inner surface of FTO panel, and the P_{out}. So, there is room for the design of networks of nanogenerators with harmonious integration into buildings without breaking the overall

aesthetics, and with different ratios of transparency and electrical power obtained by the harvesting NIR energy of outdoor sunlight and MIR energy from ambient.

4. Conclusions

In this work, by means studying the surface morphology, crystal structure, chemical composition and optical properties of the electrodeposited in the pulsed mode one-dimensional ZnO arrays and uncoated FTO substrate we were able to explain the distinguishable temperature gradients ΔT between 1-D ZnO array and uncoated FTO that are spontaneously created under heating of ZnO/FTO compositions, including under the influence of sunlight. After that, we have developed and successfully tested a new design of semi-transparent ZnO/FTO solar thermoelectric nanogenerator, which is low cost and easy to manufacture, and has long-term durability. The developed NG combines benefits of low thermal emittance of FTO and ZnO coatings with TE technology for the harvesting of photo-thermal energy of outdoor sunlight by the windows themselves to produce electricity. We have proposed a network of the developed semi-transparent nanogenerators that can be located directly on the inner surface of the Low-E windows and therefore will not interfere with cleaning the glazing. The design allows the implementing of different ratios of transparency and output electrical power. This network of NGs can serve as a source of electricity sufficiently high to make sensors wholly autonomous in energy by the harvesting NIR energy of outdoor sunlight and heat from ambient.

Conflicts of interest

There are no conflicts of interest.

References

Anderson, A.-L., Chen, S., Romero, L., Top, I., Binions, R., 2016. Thin films for advanced glazing applications. Buildings 6 (3), 37. https://doi.org/10.3390/buildings6030037 34 p.

Dongol, M., El-Denglawey, A., Abd El Sadek, M.S., Yahia, I.S., 2015. Thermal annealing effect on the structural and the optical properties of Nano CdTe films. Optik 126, 1352–1357.

He, M., Lin, Y.-J., Chiu, C.-M., Yang, W., Zhang, B., Yun, D., Lin, Z.-H., 2018. A flexible photo-thermoelectric nanogenerator based on MoS_2/PU photothermal layer for infrared light harvesting. Nano Energy 49, 588–595.

Fruh, W., Musleh, M.A., 2015. Demonstration of thermoelectric glass. Int. J. Electr. Energy 3 (4), 248–251.

Ishibe, T., Tomeda, A., Watanabe, K., Kamakura, Y., Mori, N., Naruse, N., Mera, Y., Yamashita, Y., Nakamura, Y., 2018. Methodology of thermoelectric power factor enhancement by controlling nanowire interface. ACS Appl. Mater. Interfaces 10 (43), 37709–37716.

Ito, Y., Mizoshiri, M., Mikami, M., Kondo, T., Sakurai, J., Hata, S., 2017. Fabrication of thin-film thermoelectric generators with ball lenses for conversion of near-infrared solar light. Jpn. J. Appl. Phys. 56 06GN06-1–06GN06-5.

Jao, Y.-T., Li, Y.-C., Xie, Y., Lin, Z.-H., 2017. A self-powered temperature sensor based on silver telluride nanowires. ECS J. Solid State Sci. Technol. 6 (3), N3055–N3057.

Kahouli, M., Barhoumi, A., Bouzid, A., Al-Hajry, A., Guermazi, S., 2015. Structural and optical properties of ZnO nanoparticles prepared by direct precipitation method. Superlatt. Microstruct. 85, 7–23.

Klochko, N.P., Klepikova, K.S., Tyukhov, I.I., Myagchenko, Y.O., Melnychuk, E.E., Kopach, V.R., Khrypunov, G.S., Lyubov, V.M., Kopach, A.V., Starikov, V.V., Kirichenko, M.V., 2015. Zinc oxide–nickel cermet selective coatings obtained by sequential electrodeposition. Sol. Energy 117, 1–9.

Klochko, N.P., Klepikova, K.S., Kopach, V.R., Tyukhov, I.I., Zhadan, D.O., Khrypunov, G.S., Petrushenko, S.I., Dukarov, S.V., Lyubov, V.M., Kirichenko, M.V., Khrypunova, A.L., 2018a. Semitransparent *p*-CuI and *n*-ZnO thin films prepared by low temperature solution growth for thermoelectric conversion of near-infrared solar light. Sol. Energy 171, 704–715.

Klochko, N.P., Klepikova, K.S., Petrushenko, S.I., Kopach, V.R., Khrypunov, G.S., Zhadan, D.O., Dukarov, S.V., Lyubov, V.M., Kirichenko, M.V., Surovitskiy, S.V., Khrypunova, A.L., 2018b. Influence of UV light of extraterrestrial solar irradiance on structure and properties of ZnO films prepared through pulsed electrochemical deposition and via SILAR method. J. Nano- Electron. Phys. 10 (6) 06038-1–06038-13.

Klochko, N.P., Kopach, V.R., Tyukhov, I.I., Zhadan, D.O., Klepikova, K.S., Khrypunov, G.S., Petrushenko, S.I., Lyubov, V.M., Kirichenko, M.V., Dukarov, S.V., Khrypunova, A.L., 2018c. Metal oxide heterojunction (NiO/ZnO) prepared by low temperature solution growth for UV-photodetector and semi-transparent solar cell. Sol. Energy 164, 149–159.

Kooti, M., Naghdi Sedeh, A., 2013. Microwave-assisted combustion synthesis of ZnO nanoparticles. J. Chem ID 5620281-1–ID 5620281-4.

Kopach, V.R., Klepikova, K.S., Klochko, N.P., Tyukhov, I.I., Khrypunov, G.S., Korsun, V.E., Lyubov, V.M., Kopach, A.V., Zaitsev, R.V., Kirichenko, M.V., 2016. Solar active Ag/ZnO nanostructured arrays obtained by a combination of electrochemical and chemical methods. Sol. Energy 136, 23–31.

Kumar, H., Rani, R., 2013. Structural and optical characterization of ZnO nanoparticles synthesized by microemulsion route. Int. Lett. Chem. Phys. Astron. 19, 26–36.

Litvinenko, S., Ilchenko, L., Kaminski, A., Kolenov, S., Laugier, A., Smirnov, E., Strikha, V., Skryshevsky, V., 2000. Investigation of the solar cell emitter quality by LBIC-like image techniques. Mat. Sci. Eng. B 71, 238–243.

Liu, Z., Zhang, L., Gong, G., Li, H., Tang, G., 2015. Review of solar thermoelectric cooling technologies for use in zero energy buildings. Energy Build. 102, 207–216.

Matsuo, H., Yoshitoku, K., Saito, M., Takahashi, H., Terasaki, I., Homma, T., 2018. Fabrication of ZnO-based thermoelectric micro-devices by electrodeposition. J. Electrochem. Soc. 165 (9), D417–D422.

Morishige, K., Kittaka, S., Moriyasu, T., Morimoto, T., 1980. Thermal desorption study of surface hydroxyls on ZnO. J. Chem. Soc., Faraday Trans. 1: Phys. Chem. Condens. Phases 76, 738–745.

Norouzi, M., Kolahdouz, M., Ebrahimi, P., Ganjian, M., Soleimanzadeh, R., Narimani, K., Radamson, H., 2016. Thermoelectric energy harvesting using array of vertically aligned Al-doped ZnO nanorods. Thin Solid Films 619, 41–47.

Poulek, V., Matuška, T., Libra, M., Kachalouski, E., Sedláček, J., 2018. Influence of increased temperature on energy production of roof integrated PV panels. Energy Build. 166, 418–425.

Prieto, A., Knaack, U., Auer, T., Klein, T., 2017. Solar cool facades: framework for the integration of solar cooling technologies in the building envelope. Energy 137, 353–368.

Sarbu, I., Dorca, A., 2017. A comprehensive review of solar thermoelectric cooling systems. Int. J. Energy Res. 42 (2), 395–415.

Soni, B.H., Deshpande, M.P., Bhatt, S.V., Garg, N., Chaki, S.H., 2013. Studies on ZnO nanorods synthesized by hydrothermal method and their characterization. J. Nano-Electron. Phys. 5 (4) 04077-1–04077-6.

Sowri Babu, K., Ramachandra Reddy, A., Sujatha, C., Venugopal Reddy, K., Mallika, A.N., 2013. Synthesis and optical characterization of porous ZnO. J. Adv. Ceram. 2 (3), 260–265.

Tainoff, D., Proudhom, A., Tur, C., Crozes, T., Dufresnes, S., Dumont, S., Bourgault, D., Bourgeois, O., 2018. Thermoelectric nanogenerator networks: a viable source of power for autonomous wireless sensors. J. Phys.: Conf. Ser. 1052 012138-1–012138-2.

Xiong, G., Pal, U., Serrano, J.G., Ucer, K.B., Williams, R.T., 2006. Photoluminescence and FTIR study of ZnO nanoparticles: the impurity and defect perspective. Phys. Stat. Sol. (c) 3 (10), 3577–3581.

Yang, Y., Pradel, K.C., Jing, Q., Wu, J.M., Zhang, F., Zhou, Y., Zhang, Y., Wang, Z.L., 2012a. Thermoelectric nanogenerators based on single Sb-doped ZnO micro/nanobelts. ACS Nano 6 (8) 6984-1–6984-9.

Yang, Y., Guo, W., Pradel, K.C., Zhu, G., Zhou, Y., Zhang, Y., Hu, Y., Lin, L., Wang, Z.L., 2012b. Pyroelectric nanogenerators for harvesting thermoelectric energy. Nano Lett. 12 (6), 2833–2838.

Zak, A.K., Majid, W.H.A., Abrishami, M.E., Yousefi, R., 2011. X-ray analysis of ZnO nanoparticles by Williamson-Hall and size–strain plot methods. Solid State Sci. 13, 251–256.

Zappa, D., Dalola, S., Faglia, G., Comini, E., Ferroni, M., Soldano, C., Ferrari, V., Sberveglieri, G., 2014. Integration of ZnO and CuO nanowires into a thermoelectric module. Beilstein J. Nanotechnol. 5, 927–936.

Zhan, T., Yamato, R., Hashimoto, S., Tomita, M., Oba, S., Himeda, Y., Mesaki, K., Takezawa, H., Yokogawa, R., Xu, Y., Matsukawa, T., Ogura, A., Kamakura, Y., Watanabe, T., 2018. Miniaturized planar Si-nanowire micro-thermoelectric generator using exuded thermal field for power generation. Sci. Technol. Adv. Mater. 19 (1), 443–453.